**Electronic Supplementary Information (ESI)**

# Integrated Architecture for the Electrical Detection of Plasmonic Resonances Based on High Electron Mobility Photo-Transistors

**Davide Sammito,[a,b] Davide De Salvador,[c] Pierfrancesco Zilio,[a,c] Giorgio Biasiol,[b] Tommaso Ongarello,[a,c] Michele Massari,[a] Gianluca Ruffato,[a,c] Margherita Morpurgo,[d] Davide Silvestri,[d] Gianluigi Maggioni,[c,e] Gianluca Bovo,[c] Michele Gaio[c] and Filippo Romanato[a,b,c]**

[a] *Laboratory for Nanofabrication of Nanodevices, LaNN - Veneto Nanotech, Corso Stati Uniti 4, 35127 Padova, Italy. E-mail: davide.sammito@venetonanotech.it*
[b] *Istituto Officina dei Materiali, IOM - CNR, SS. 14 km 163.5 in Area Science Park, 34149 Basovizza (Trieste), Italy.*
[c] *University of Padova, Department of Physics and Astronomy, Via Marzolo 8, 35131 Padova, Italy. E-mail: davide.desalvador@unipd.it*
[d] *University of Padova, Department of Pharmaceutical and Pharmacological Sciences, Via Marzolo 5, 35131 Padova, Italy*
[d] *INFN Legnaro National Laboratories, Viale dell'Università 2, 35020 Legnaro (Pd), Italy*

## HEMTs optical response

In the following the electro-optical characteristics of the developed HEMT are reported. In order to verify that the optical response of our devices is consistent with models of photo-HEMTs operation presented in literature, we reproduced the characterization procedure and used the analytical models proposed by Takanashi *et al.*[1]. They reported an increase of drain current with illumination in InAlAs/InGaAs HEMTs and explained this phenomenon by an effective decrease in the potential barrier for electrons between the source and the channel due to the photovoltaic effect.

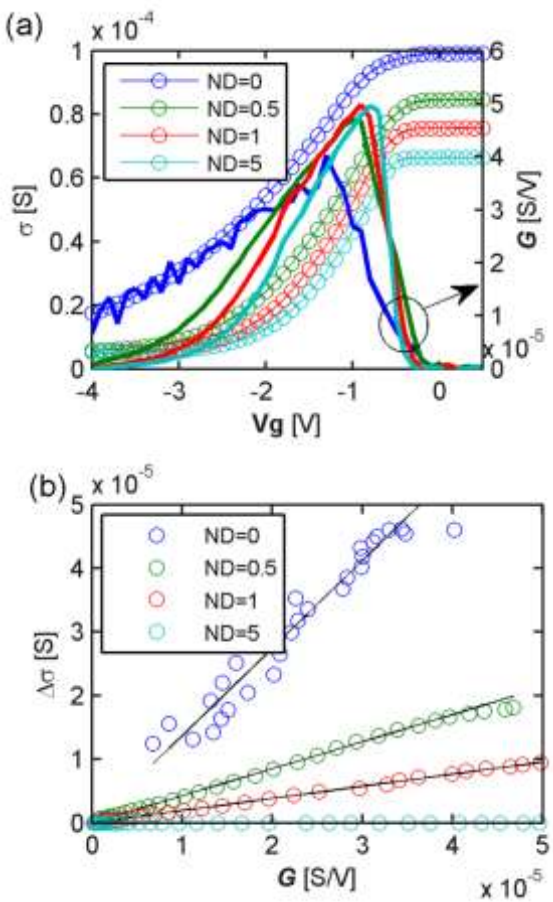


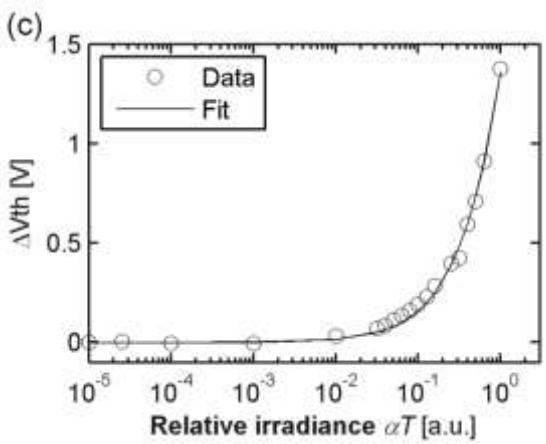


**Fig. S1** (a) Conductance $\sigma$ (dotted lines) and $G = d\sigma/dVg$ (solid lines) versus gate voltage *Vg* for different Neutral Density (ND) filters applied to attenuate the irradiance incident on the device (1 mW non-attenuated laser power). (b) Variations of conductance, compared to dark conditions, versus *G* for different relative irradiance values. (c) Shift of the transistor threshold voltage as a function of the relative incident irradiance and corresponding fit by equation (S1).

Driving the device with a fixed source-drain current (*Ids*) and gate-source voltage (*Vg*), we measure an increase of channel conductance $\sigma$ with illumination, which is equivalent to a reduction of the threshold voltage of the transistor ($\Delta Vth$). This is shown in Fig. S1a where $\sigma$ is plotted (dotted lines) as a function of *Vg* for different optical powers, expressed by the attenuation factor $\alpha = 10^{-ND}$ of the incident laser beam (1 mW) applied by Neutral Density (*ND*) filters. In the same graph we report the trend of $G = d\sigma/dVg$ (solid lines), which is the equivalent to the transconductance driving the device by a known source-drain voltage instead of current. Since $\sigma$ is a function of *Vg-Vth*, it can be shown[1] that the shift of the threshold voltage, compared to dark conditions, is obtained by a linear fit of the conductance variations versus *G* (Fig. S1b), for *Vg* values close to *Vth*.

Finally we fit the data of threshold voltage variation versus relative irradiance (Fig. S1c) by an analytical model[1], which assumes a linear relationship between $\Delta Vth$ and the open-circuit potential caused by the accumulation of photogenerated holes at the source:

$$\Delta Vth = n\frac{kT}{q}\ln\left(1+\frac{\eta qP}{I_d h\nu}\right) \quad \text{(S1)}$$

where $n$ is an empirical proportionality factor, $kT/q$ is the thermal voltage, $\eta$ is the quantum efficiency associated with the absorption process in the GaAs channel, $h\nu$ is the photon energy, $I_d$ is the dark current for holes, $q$ is the electron charge and $P$ is the optical power. As can be seen in Fig. S1c, the model satisfactorily describes the data acquired on our devices.

## Device fabrication flow chart

We realized, by lithographic techniques, devices for four point probe measurement of 2DEG conductance under illumination. We chose a Hall bar layout, by which also electron population and mobility can be obtained by applying a magnetic field, even if, for biosensing purpose, only the resistance measurement has been used. The Hall bars consists of MESA structures etched in the epitaxial multilayer in order to electrically isolate 2DEGs belonging to different devices present on the same chip. Metallic pads on the MESA, forming ohmic contacts with the 2DEG, are used for the electrical contacts of source, drain, $V_+$ and $V_-$ (Fig. 1b). An additional pad is needed for the gold lead that simultaneously works as nanostructured plasmonic surface and electronic gate of the transistor: this gold layer crosses the central arm of the device, covering the grating etched in the GaAs cap in the active area (dark red area in Fig. 1b), and forms a Schottky contact.

We fabricated two batches of these devices with slightly different layouts. The first one has a squared active area (500x500 $\mu m^2$) while the second one has a rectangular active area (60x240 $\mu m^2$). One chip of the device is made of two active areas sharing the gate contact pad (only one active area is shown in Fig. 1b). The fabrication flow chart is made up of several steps: three aligned optical lithographies (MESA, contacts, gate); one electron beam lithography nanopatterning (grating) aligned with the microstructures; two wet etching processes (MESA, V-groove grating); two e-gun evaporations in vacuum (metallization, gate) followed by lift-off. Hereafter we will briefly describe the designed flow chart.

After cleaning in organic solvents the epitaxial samples grown by MBE, the first step is the UV-optical lithography of the MESA structures. We used Shipley S1818 (1.9 µm-thick) as optical photoresist. The micro-pattern is aligned along the principal crystallographic orientations using wafer's flats. In particular the main channel between source and drain, along which *Ids* flows, is oriented normal to the $[01\bar{1}]$ direction, along which the V-grooves are aligned. The resist pattern is used as mask for the wet etching process, performed in a $H_3PO_4$:$H_2O_2$:$H_2O$ solution in ratio 3:1:50 by volume, at room temperature. This solution etches both GaAs and $Al_{0.42}Ga_{0.58}As$ at a rate of about 100 nm/s. The etching process is stopped, by rinsing in de-ionized water, at a thickness (~900 nm) greater than the 2DEG depth and lower then the superlattice depth. Thus, at the end of the MESA etching phase, Hall bar devices are in relief while the surrounding surface is etched down to the GaAs epi-layer. The undercut below the resist mask is negligible compared to MESA dimensions. Alignment marks necessary for the following optical and Electron Beam Lithography (EBL) steps are also realized in this step.

For the contacts definition step, a lift-off resist (LOR7B, 700 nm-thick) is spun before the optical photoresist. Contact areas are opened on the MESA structures. The GaAs surface of the contact areas is deoxidized by a 5'' dip in diluted HCl and dried via nitrogen blow, just prior to the loading of the sample in the evaporation chamber. A nickel\germanium\gold tri-layer (20\60\130 nm-thick) is deposited by e-beam evaporation at a deposition rate of 0.1 nm/s. The Ni layer improves the adhesion to the surface and the Au layer reduces contact resistance, while the Ge layer allows the contacts to diffuse into the sample when annealed. After the lift-off in an ultrasonic bath of acetone first and resist developer (MF319) then, the sample is rinsed in methanol and the annealing process is performed. Ohmic contacts are made by placing the sample on a copper strip, heated by Joule effect up to the temperature of 420° for about 1', in nitrogen atmosphere.

The V-groove grating is integrated on the active area by EBL nanopatterning followed by anisotropic GaAs wet etching. PMMA (AR-P 671.05, 490 nm-thick) is used as electron beam resist. Periodically spaced 70 nm-wide lines are exposed by a 100 keV electron beam having a current of 2 nA and with a dose of about 860 $\mu C/cm^2$. The EBL apparatus is a Jeol JBX-6300FS situated at LaNN Laboratory (Veneto Nanotech) in Padova. It is able to automatically identify the markers realized by UV lithography and to align the exposures on the Hall bars and, thus, respect to the crystallographic axes. The samples are developed for 1' in $H_2O$:IPA 3:7 and rinsed in DI water.

A variety of etchants has been reported for GaAs crystals, most of them being anisotropic because of the different surface activity of Ga- and As-terminated planes[2–5]. In particular, several solutions based on acids – hydrogen peroxide mixtures work as crystallographic orientation-dependent etchants. We use a solution of $H_2SO_4$:$H_2O_2$:$H_2O$ 1:8:40 by volume for 25''. The PMMA mask endure this dilute etching process, which creates a significant undercut below resist stripes. The resist is stripped in acetone after etching. The anisotropy of the etching exposes groove sidewalls in the {111}A orientations that, for optimal etching conditions, meet with sharp corners at the bottom of the structure, thus forming an array of V-shaped grooves.

Another UV lithography step is performed to pattern the gate contact. A LOR7B\S1818 bi-layer is spun, exposed and developed. Samples are then loaded in the vacuum chamber for e-gun evaporation of a 180 nm-thick gold layer on top of a thin (3 nm) titanium adhesion layer (deposition rates 0.05 nm/s). After the final lift-off step, the V-groove grating on the active area is conformally coated by gold (Fig. 4a) and electrically connected to the central lead (on the bottom in Fig. 1b), by which it is possible to bias the gate.

Finally the samples are cut and the dies are glued on sockets by a bi-component epoxy resin. Electrical connections between the socket and the pads on the die are realized by a wedge bonder equipment and 12 µm-thick Au wires (Fig. S2).

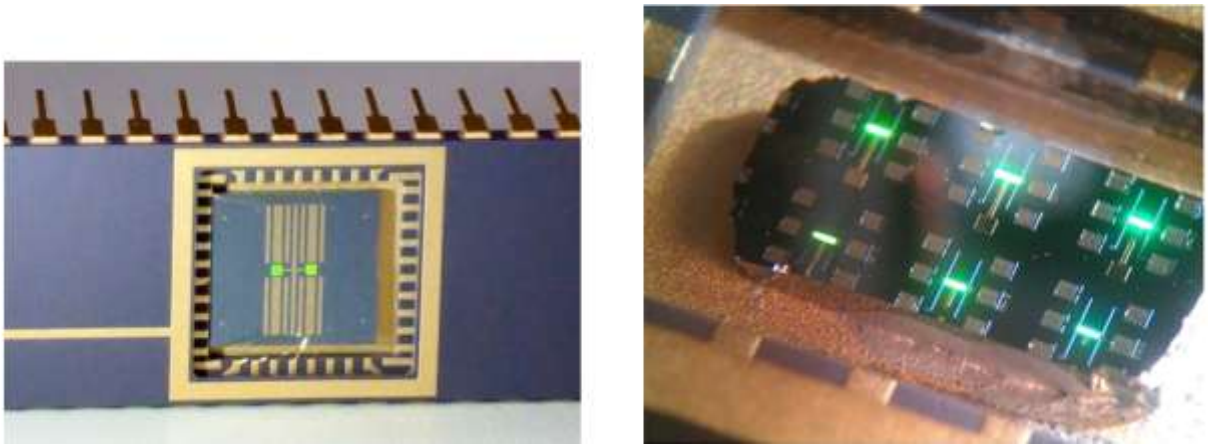

**Fig. S2** Pictures of two dies bonded to sockets and belonging to the first batch (left) and to the second batch (right) of devices.

## Estimate of device resolution based on numerical simulations

The sensitivity of the device in terms of film thickness ($t$) coating the gold grating can be expressed as the derivative of the measured quantity (conductance) with respect to the film thickness. Given the logarithmic electro-optical response of the device, equation (2), the sensitivity is calculated as

$$S_t = \frac{\partial \sigma}{\partial t} = m_\sigma \cdot \frac{1}{T}\frac{\partial T}{\partial t} \qquad \text{(S2)}$$

In order to estimate $S_t$, we get $m_\sigma$ from experimental data (~$3.7\cdot10^{-5}$ $\Omega^{-1}$, Fig. 2b) and we calculate by FEM simulations the transmittance ($T$) for the optimal plasmonic grating configuration as a function of the thickness of a 1.45-refractive index coating layer. This last procedure is supposed to be quite accurate given the validation of the device simulation reported in Fig. 6. In Fig. S3 we report the transmittance as a function of $t$ as well as its derivative divided by $T$ in the case of the optimal structure described in the main text (period = 628 nm, groove width = 364 nm).

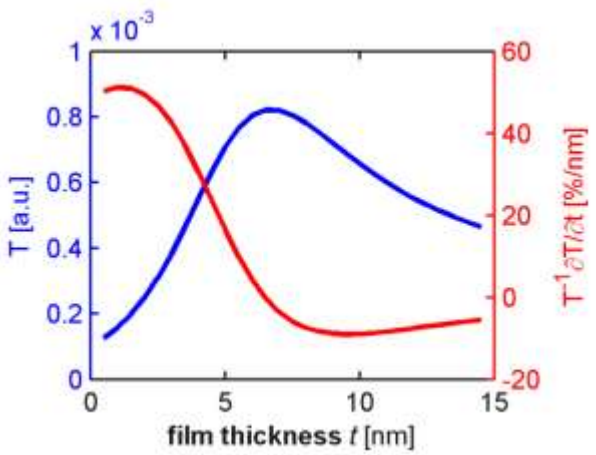


**Fig. S3** Transmittance $T$ and $T^{-1}\partial T/\partial t$ as a function of the film thickness $t$ (refractive index 1.45) for the optimal configuration of triangular groove array (period = 628 nm, slit/period = 0.58).

As can be noted the maximum sensitivity is achievable for a coating thickness of few nanometers and amounts to about $\boldsymbol{S_t}$**=1.9·10$^{-5}$ Ω$^{-1}$/nm**[*]. Moreover, the *resolution* of the sensor (i.e. the smallest change of a measurand which produces a detectable change in the sensor output[6]) can be estimated. In our case it is given by

$$R_t = \frac{\partial t}{\partial \sigma}\delta_\sigma = \frac{\delta_\sigma}{S_t} \qquad \text{(S3)}$$

where $\delta_\sigma$ is the experimental error on the conductance measurement. The signal fluctuations are affected by the electronic noise and the laser stability. $\delta_\sigma$ has been measured performing multiple consecutive angular scans and estimated to be ~$3\cdot10^{-7}$ $\Omega^{-1}$. Finally, an estimate of the sensor theoretical resolution is $\boldsymbol{R_t \approx 1.6\cdot10^{-2}}$ **nm.**

The reported values of sensitivity and resolution are connected to the specific refractive index adopted for the layer. In order to provide more general figures of merit for the sensor performance evaluation, the sensitivity and resolution are usually reported in terms of Refractive Index Unit (RIU) instead of thickness of a specific kind of layer. More in detail, the detector response variation is evaluated by varying the index of refraction of the whole (bulk) dielectric space in contact to the metal, $n_{eff}$ (effective index). The latter is calculated by FEM simulations, obtaining the transmittance and its derivative as a function of $n_{eff}$ (Fig. S4). By these data the sensitivity can be obtained as:

$$S_{eff} = \frac{\partial \sigma}{\partial n_{eff}} = m_\sigma \cdot \frac{1}{T}\frac{\partial T}{\partial n_{eff}} \qquad \text{(S4)}$$

[*] It is worth to note that the optimal structure is not obtained maximizing the sensitivity in this differential form but in a discrete formulation, where the relative transmittance variation is obtained by the difference of transmittance with and without a 5 nm-thick layer. This choice causes a minor variation of the optimal geometric parameters that it is lower than the dimensional inaccuracy in the fabrication of the designed nanostructures.

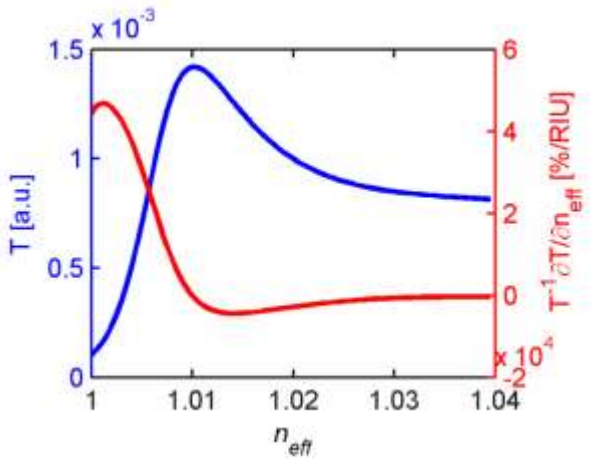


**Fig. S4** Transmittance $T$ and $T^{-1}\partial T/\partial\ n_{eff}$ as a function of the effective refractive index for the optimal configuration of triangular groove array (period = 628 nm, slit/period = 0.58).

The maximum calculated relative transmittance variation, $T^{-1}\partial T/\partial n_{eff}$, for the present configuration is about 46000 %/RIU (Fig. S4). Considering equation (S4), defining the sensitivity of the device, we can finally estimate $\boldsymbol{S_{eff}}$**≈ 1.7·10$^{-2}$ Ω$^{-1}$/RIU**. The relative sensor theoretical resolution in terms of RIU can thus be calculated by using

$$R_{eff} = \frac{\partial n_{eff}}{\partial \sigma}\delta_\sigma = \frac{\delta_\sigma}{S_{eff}} \qquad \text{(S5)}$$

obtaining $\boldsymbol{R_{eff}}$**≈1.8·10$^{-5}$ RIU**.

## Synthesis of thiolated biotin: 5-(2-oxo-hexahydro-1H-thieno[3,4-d]imidazol-4-yl)-N-(6-(3-(tritylthio) propanamido)hexyl)pentanamide

A thiolated derivative of biotin was synthesized to functionalize the gold surface and test the device as an affinity biosensor (see the following section). 100 mg of biotinylamidohexanolamine (Biotin-$(C_2)_6$-$NH_2$ - 0.29 mmol) were dissolved in 5 ml anhydrous N-Methyl-2-pyrrolidone (NMP) and 101.8 mg S-tityl-3-mercaptopropionic acid ((trt)MPA – IRIS biotech; 1 eq.), 33.63 mg N-hydroxysuccinimide (NHS – ACROS; 1 eq.) and 66.3 mg diciclohexylcarbodiimide (DCCI – Sigma; 1.1 eq.) were added, the pH was immediately adjusted to ~8.5 with triethylamine (TEA - Sigma). The reaction was followed with ninhydrin observing the disappear of the amine-related purple spot; after 1h the precipitated diciclohexylurea (DCU) was removed by gooch filtration and the product precipitated in diethyl ether; the product was recovered with anhydrous methanol, and the presence of biotin assessed with Renz & Loew reactive[7] (red-purple spot on TLC). 3 ml of methanolic solution, corresponding to 57 mg of product, were divided into aliquots, dried in vacuum and stored under inert gas at -20°C.

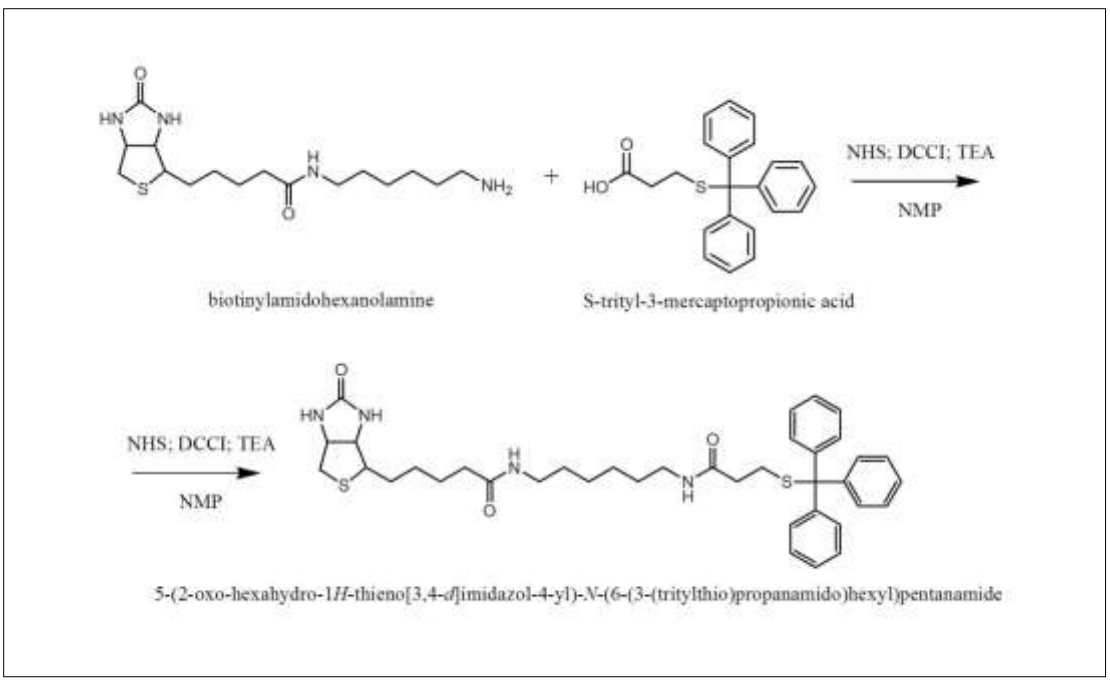


**Scheme S1** General scheme of thiolated biotin derivative.

## Biotin functionalization and avidin binding procedure

We tested the device operation as an affinity biosensor with a well known biochemical interaction, the binding of avidin to biotin, featuring a high specificity and affinity constant[8–10]. The samples were cleaned with multiple rinses in ethanol and pre-characterized with the bare gold surface. Then a 2 mM ethanolic solution of a thiolated biotin derivative was prepared from aliquots previously prepared (see precedent section): the trityl protecting group was removed dropping trifluoroacetic acid (15-20 µl/0.5 ml final solution) on the ppt; after 15 min the TFA was evaporated in vacuum for 10 min and ethanol was added to the

final volume; few drops (~50 µl) of the solution were deposited on the samples and kept in an ethanol-saturated atmosphere for 16 hours. Further rinses in ethanol were performed to wash away biotin molecules not stably bonded to the gold active area by the Au-S bond. The phototransistors response was characterized after this functionalization step too. Finally few tens micro-litres of 4 µg/ml avidin in DI water solution were applied on the surfaces for 15' and the samples were rinsed in water to wash un-bound avidin molecules away.

## Notes and references


1. Y. Takanashi, K. Takahata, and Y. Muramoto, *IEEE Electron Device Letters*, 1998, **19**, 472–474.
2. X. Wang, *Journal of Crystal Growth*, 2000, **213**, 19–26.
3. S. Adachi and K. Oe, *Journal of The Electrochemical Society*, 1983, **130**, 2427.
4. S. Sioncke, D. P. Brunco, M. Meuris, O. Uwamahoro, J. Van Steenbergen, E. Vrancken, and M. M. Heyns, *ECS Transactions*, 2008, **16**, 451–460.
5. S. W. Tan, M. K. Hsu, a H. Lin, M. Y. Chu, W. T. Chen, and W. S. Lour, *Semiconductor Science and Technology*, 2004, **19**, 384–388.
6. J. Homola, Ed., *Surface Plasmon Resonance Based Sensors*, Springer Berlin Heidelberg, Berlin, Heidelberg, 2006, vol. 4.
7. C. Renz and K. Loew, *Berichte der deutschen chemischen Gesellschaft*, 1903, **36**, 4326–4330.
8. M. Wilchek and E. A. Bayer, *Methods Enzymol*, 1990, **184**, 5–13.
9. M. Wilchek and E. A. Bayer, *Methods Enzymol*, 1990, **184**, 467–9.
10. M. Wilchek, E. A. Bayer, and O. Livnah, *Immunol Lett*, 2006, **103**, 27–32.